Smart Power Unit—mW-to-nW Power Management and Control for Self-Sustainable IoT Devices

Philipp Mayer, *Student Member, IEEE*, Michele Magno, *Senior Member, IEEE*, and Luca Benini, *Fellow, IEEE*

***Abstract*—Self-sustainability and intelligence will be critical features of the next generation of Internet of Things devices. Power management circuits need to be energy-efficient in multiple power modes, from nW sleep to mW active, and to support energy harvesting (EH) from multiple environmental sources. This article presents an adaptive and firmware-configurable power supply unit that enables intelligent devices to operate in the sub μW range while achieving self-sustainability through EH. The microcontroller-based design allows efficient conversion from batteries, dc, ac environmental sources, and nA quiescent currents. Source and load power points are decoupled with multiple dc–dc converters aiming to supply loads with adaptive voltage scaling and achieving high reliability. Experimental results show the flexibility and efficiency of this approach: the proposed power supply unit achieves a quiescent current of 54 nA and a maximum peak load current of 300 mA, delivered with an end-to-end power efficiency above 85%.**

***Index Terms*—Energy efficiency, energy harvesting, energy management, event detection, Internet of Things, sensor systems and applications.**

I. Introduction

LOW power wireless smart sensors are playing a crucial role in the development of the Internet of Things (IoT). These intelligent devices are planned to be utilized for a wide range of applications aimed at monitoring industrial and civil structures and environments, such as autonomous operated access control systems and condition monitoring for industrial machinery, among others [1]. However, the main obstacle for such intelligent devices, and in general for IoT devices, to become truly pervasive is their need for a long-term reliable power source. The use of batteries is the most direct way of powering wireless devices, but regular battery replacement is vital to ensure continuous operation. Such a requirement is unappealing as it implies high maintenance costs, especially in remote areas or if environmental issues related to battery disposal are of concern [2]. Moreover, in applications where IoT devices are deployed in a large number (i.e., thousands or more), battery replacement might result inconvenient or even not possible. Predictions for wireless sensors to enable the IoT show a two-fold increase between 2018 and 2023, which will result in a significantly higher demand for power sources to supply an estimated 50 billion wireless sensors [3]. Therefore, finding a convenient solution to supply this massive amount of devices perpetually is a highly topical research subject [1].

Energy harvesting (EH), the technology to convert energy from environmental sources, is the most promising technology to achieve perpetually powered sensors for the IoT, with zero battery replacements over their mission lifetime. EH is already a mature technology for both commercial and residential settings [4]. However, many challenges are still open for tiny-form factor harvesters, needed for the majority of unobtrusive smart sensors [5]. Moreover, by opting for an EH source, additional circuitry, and energy management (EM) techniques are required when compared with main-power and battery-powered solutions. In particular, this auxiliary circuit is essential, due to the low-power, low-voltage nature of small form factor EH sources and the significant power profile mismatch between the source and the load. For this reason, a dc-dc converter, an EM circuit, and energy storage are required between the EH source and a wireless sensor load, as shown in Fig. 1.

In the aforementioned IoT context, smart sensors are usually wirelessly exchanging information with other sensors or remote hosts. One major trend is "near-sensor" processing, which allows shifting from "raw data" transmission towards "information" transmission, thereby reducing communication bandwidth and costs [6]. However, this comes with an additional challenge for power supply design, namely the need to support an extremely wide range of active power consumption. Novel microcontrollers for near-sensor processing, exploiting near-threshold operation [7] and high parallelism [8], achieve GOp/s performance but have active power delivery requirements ranging from hundreds of μW to tens of mW. Additionally, emerging wireless communication technologies such as Long Range (LoRa) with a peak consumption of tens of mW or Narrowband Internet of Things (NB-IoT) and Ultra Wide Band (UWB) with up to hundreds of mW impose even more demanding requirements on the sensors supply power delivery range, [9], [10].

A third challenge to perpetual operation is the need to support extremely aggressive Duty Cycling (DC), i.e., switching-off

Manuscript received February 7, 2020; revised June 16, 2020 and August 25, 2020; accepted October 3, 2020. Date of publication October 16, 2020; date of current version January 22, 2021. This work was supported by the Office of Naval Research Global Grant "Zero-Power Sensing for Underwater Monitoring"under Grant 62909-19-1-2018. Recommended for publication by Associate Editor J. A. Cobos. *(Corresponding author: Philipp Mayer.)*

Philipp Mayer is with the Integrated Systems Laboratory, ETH Zurich, 8092 Zurich, Switzerland (e-mail: mayerph@iis.ee.ethz.ch).

Michele Magno is with the Center for Project-Based Learning, ETH Zurich, 8092 Zurich, Switzerland (e-mail: michele.magno@iis.ee.ethz.ch).

Luca Benini is with the Integrated Systems Laboratory, ETH Zurich, 8092 Zurich, Switzerland, and also with the Department of Electrical, Electronic and Information Engineering, University of Bologna, 40136 Bologna, Italy (e-mail: luca.benini@unibo.it).

Color versions of one or more of the figures in this article are available online at https://ieeexplore.ieee.org.

Digital Object Identifier 10.1109/TPEL.2020.3031697

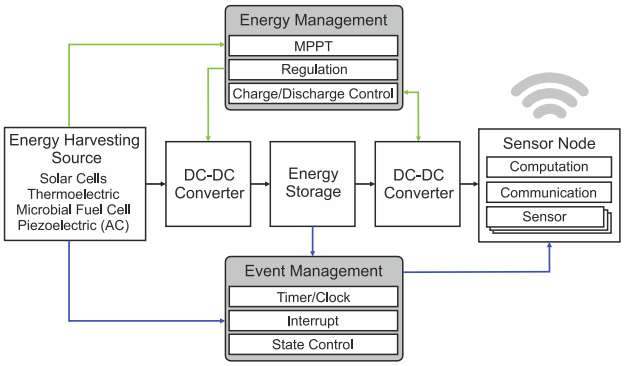

Fig. 1. System overview of an EH-powered smart sensor node for the IoT.

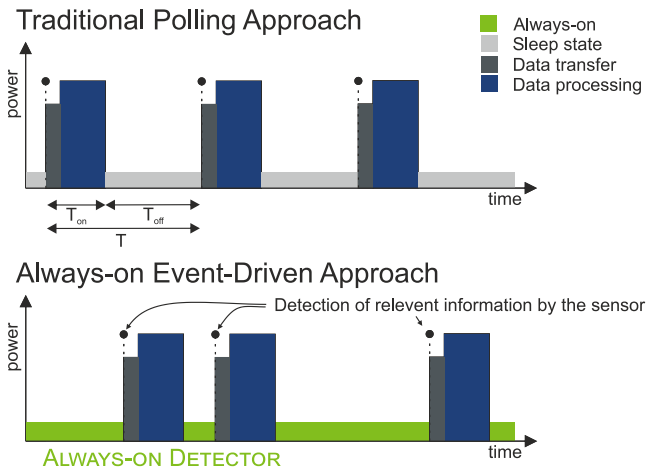

Fig. 2. Traditional duty cycling approach where the system is off for a predetermined period (T_{off}) to save energy and activated for a small portion of time T_{on} versus always-on event-driven approach where an ultra-low-power detector is continuously processing the information to detect relevant events before waking up the full sensing system.

subsystems when they are not needed. DC enables matching low and fluctuating harvested power with the load requirements during active operation, even though such matching requires close co-design of the energy management with the EH source and system load. In particular, this includes an application-specific analysis of the applicability of EH, energy statistics, and an adequate sizing of the energy storage element. In general, DC reduces the overall power consumption, but it also deactivates parts of the system, which could lead to the loss of events [11], [12]. The upper part of Fig. 2 shows the DC/polling approach where the system is put in a deep-sleep mode for a predetermined period (T_{off}) to save energy and is activated only for a short time interval (T_{on}). This time-triggered operation results also in a trade-off between average power reduction and latency and can ultimately lead to missed events for long-off durations. The lower part of Fig. 2 shows an approach to overcome this drawback of baseline DC. In particular, a part of the sensing system is always-on to detect events of interest (event-triggered DC) switching to the higher power part only when necessary. One of the most important features of the always-on sub circuitry is to consume order-of-magnitude lower power than the entire sensing system in active mode [13], [14].

The requirement of supporting always-on circuits for sensing (needed for event-triggered DC) and for state retention (needed for both time-triggered and even-triggered DC) further extends the range of power levels that need to be efficiently supported by the power supply subsystem.

This work addresses the challenge of achieving high energy efficiency across operating states that have wide-ranging power requirements, spanning six orders of magnitude, from tens of mW to tens of nW [1]. The paper propose smart power supply architecture for energy-proportional IoT intelligent sensing systems, which can scale their detection accuracy together with the power consumption to achieve perpetual operation without compromising latency and accuracy [15]–[18]. The smart power unit is designed to harvest energy from multiple environmental resources with the target of high energy efficiency.

The main contribution of this article is the architecture and design of a heterogeneous Smart Power Unit (SPU), which combines state-of-art low power integrated circuits (ICs), novel architecture, and low-power design techniques. The control and power management circuit allows great versatility, without utilizing resource-intensive processing, enabling the system operation at sub-μA of quiescent current while providing the following functionality.

1) A multiple system voltages architecture, suitable for operating sub-circuits such as RF modules, sensors, and microprocessors at their optimal power point.
2) An always-on power domain for retention and sensing.
3) EH from ac or dc sources with battery charge control and protection.
4) A configurable real-time clock (RTC) for time triggered operation.
5) Threshold-based wake-up capabilities for event-triggered operation.
6) Limited processing capabilities to offload lightweight tasks for longer sleep periods of the host system.

In particular, this article presents three novel contributions.

1) The design of an energy-efficient and adaptive smart power unit for self-sustainable IoT devices, which includes a software reconfigurable power management module allowing system operation in the sub µW range while supporting self-sustainability through EH.
2) A novel design for low-leakage always-on subsystem to minimize the quiescent current of the power unit, and an adaptive multi-voltage subsystem to supply the host system efficiently.
3) An accurate evaluation of the proposed smart power unit for the operating points in terms of energy efficiency, and for different application scenarios, including a comparison between the duty cycling approach (polling) and the event-triggered approach.

Finally, the proposed architecture, including the low quiescent power control circuit, is evaluated as a whole subsystem with a focus on voltage levels of conventional batteries or supercapacitors. The evaluation is performed independent of a specific harvesting source and voltage domain to demonstrate flexibility coupled with low quiescent current and high energy efficiency.

TABLE I
OVERVIEW OF THE USED ABBREVIATIONS

Abbreviations	Description
SPU	Smart Power Unit
IoT	Internet of Things
EH	Energy harvesting
EM	Energy management
LoRa	Long Range
NB-IoT	Narrowband Internet of Things
UWB	Ultra Wide Band
DC	Duty Cycling
SC	Switched capacitors
MPPT	Maximum power point tracking
FOCV	Fraction open-circuit voltage
RCC	Ripple correlation control
AIB	Analog iterating-based
IC	Integrated Circuit
LDO	Low-dropout regulator
MCU	Microcontroller unit
ADC	Analog-Digital Converter
DAC	Digital-Analog Converter
I2C	Inter-Integrated Circuit
UART	Universal Asynchronous Receiver Transmitter
GPIO	General Purpose Input-Output
RTC	Real-time clock
NVC	Negative voltage converter
FWR	Full-wave rectifier
PULP	Parallel ultra-low-power processors
ICSP	Circuit Serial Programming
SMU	Source/measurement unit
CCDF	Complementary cumulative distribution function

The energy efficiency, among other parameters, is compared with different novel circuit architectures, illustrating the benefits of the proposed solution.

The rest of the article is organized as follows: Section II presents the recent literature; Section III describes the proposed circuit; Section IV shows experimental results and possible applications. Finally, Section V concludes this article. A list of the used abbreviations is reported in Table I.

II. RELATED WORK

The literature on EH to perpetually power smart devices has been very prolific, with many examples of self-sustainable devices [1], [5], [19], [20]. One of the most important requirements in designing the EH subsystem is the low quiescent current and the high-energy efficiency of the conversion across the operation ranges, typically achieved with maximum power point tracking (MPPT) [5], [19]–[21]. A recent survey of power conversion for sensors nodes exploiting energy harvesting, including an overview of EH topologies, energy storage technologies, and algorithms is given in [1]. In [22], a power management and harvesting circuit for ac sources is presented. The implementation with off-the-shelf components allows MPPT and energy transfer features at a power envelope of tens of microwatt. Ju *et al.* [23] present a novel predictive power management framework for battery-less IoT devices, including algorithms for power point tracking, predictive energy allocation, and adaptive transmission power control. Although the simulation results suggest substantial improvements in the robustness of battery-less IoT devices, the complexity and overhead limit the application to systems with a power consumption of hundreds of mW. Shi *et al.* [24] present a power management circuit with a conversion efficiency of up to 80.6 % from a wide voltage range ac input source with a peak power consumption of 3.69 mW. The solution proposed in this article outperforms the previous works and includes more functionality, lower quiescent current and higher energy efficiency, and present a whole system with accurate measurements.

A comparison with related work in the field of integrated energy harvesting circuits is shown in Table II, differentiated in approaches operating in the sub-mW range and solutions which also support multi-mW loads. The core of these harvesting circuits are voltage converters in the topology of inductor based boost converters or inductor less in the form of switched capacitors. Source impedance matching in the μW–mW range is commonly done with the fraction open-circuit voltage approach, with some exceptions of ripple correlation control or analog iterating-based methods. In the sub-mW range, El-Damak *et al.* [25] have proposed an integrated solar EH circuit with battery management achieving a quiescent current of only 1.1 nA allowing to harvest between 10 nW and 1 μW of power without integrated MPPT circuitry. The authors in [26] presented a highly integrated EH and power management circuit with an idle current consumption down to 18 nA. The circuit allows harvesting from multiple low voltage ac or dc sources with an output power between 25 nW and 40 μW while including MPPT and load regulation circuits. One drawback of the solution presented in [26] is the limited storage voltage of only 1.5 V and the inefficient dc–dc converter consuming 30 μW when active. Furthermore, many IC optimized for higher transducer bandwidth have been presented, such as from the authors in [27] and in [17]. The proposed ICs are operating between 1 and 437 μW, respectively, 6 μW and 1.4 mW at quiescent currents of 121 nA and 2.6 μA. The stated 121 nA was achieved by excluding the load regulation circuit with 251 nA quiescent current, and at a supply voltage of only 2.0 V. Harvesting from very low voltage ac or dc sources with up to 50 mW power delivery is presented in [16]. Input voltage down to 60 mV is possible because of an active rectifier, which however raises the controller consumption to 8 μA.

Recent works show a growing effort in increasing robustness and availability by combining multiple energy harvesting transducers. In [28], a multi-input energy harvesting combiner is presented, allowing to harvest from three transducers up to 355 μW. Amin *et al.* [29] present a fully integrated power management unit with multiple transducer inputs and regulated outputs. The design allows individual MPPT and can supply loads up to 60 mW with and quiescent current down to 262 nA. Finally, in [18], a novel fully integrated energy harvesting power management unit is presented. Combining state-of-the-art features of multisource harvesting, MPPT, load regulation, and start-up circuit in a single device. It allows harvesting between 5 μW and 2.6 mW from up to four transducers with a minimum input voltage of 250 mV, respectively, 400 mV during cold start. The whole circuit achieves a typical quiescent current of 950 nA with an end-to-end efficiency of 70 %. In contrast with the previous works presented above, our work is a standalone

TABLE II
COMPARISON AGAINST STATE-OF-THE-ART HARVESTING CIRCUITS

	VLSIC'15 [25]	JSSC'16 [26]	PELS'16 [27]	TIE'18 [28]	TPE'16 [16]	TPE'19 [17]	TIE'19 [18]	**This Work**
	sub-mW				µW - mW			
EH Topology	boost ind.	boost ind.	boost ind.	SC	buck-boost ind.	SC	SC	boost ind.
Peak efficiency	84 %	87 %	77.1 %	58.4 %	72.5 %	74.6 %	70 %	90 % to battery 85 % to load
Quiescent Current	1.1 nA	18 nA	121 nA	> 3 µA	> 8.3 µA	2.6 µA	950 nA	595 nA (EH) 54 nA (deep sleep)
Power range	10 n – 1 µW	25 n – 40 µW	1 µ – 437 µW	< 355 µW	200 µ – 50 mW	6 µ – 1.4 mW	5 µ – 2.6 mW	2 µ – 200 mW
Voltage range	0.14 – 0.6 V	> 50 mV	74 m – 2.5 V	0.26 – 0.5 V	60 m – 5 V	0.8 – 5 V	> 250 mV	0.1 – 5.1 V
Startup voltage	0.33 V	0.2 V	0.22 V	0.26 V	-	0.8 V	0.4 V	0.6 V
EH inputs	1, DC	3, AC/DC	1, DC	3, DC	1, AC/DC	1, DC	4, DC	1, AC/DC
MPPT	external	FOCV	FOCV	external	AIB	simplified RCC	FOCV	FOCV
Battery voltage	2.9 – 4.1 V	typ 1.5 V	0 – 2.5 V	-	2.6 – 4.2 V	0 – 5 V	3 – 4.2 V	3.4 – 4.2 V
Load regulation	buck	LDO (Iq 30 µA)	LDO (Iq 251 nA)	no	buck	no	hybrid LDO	1x LDO, 2x buck
Technology	0.18 µm	0.18 µm	0.32 µm	0.18 µm	0.15 µm	0.18 µm	0.18 µm	-
System cost	low	low	low	very low	low	very low	very low	high
Configurability	no	no	bias signals	no	bias signals	no	bias signals	SW configurable at runtime

solution aiming to achieve high efficiency not just in a very specific and limited use case but over a wide area of applications.

The proposed circuit, based on a commercial energy harvesting IC outperforms most academic and commercial solutions in terms of input power range, and end-to-end efficiency. In addition, the circuit supports all common storage chemistries without limitation to low voltages. The combination with software configurable power management and low-power design allows us to achieve comparable or lower quiescent currents without compromising functionality and with significantly increased flexibility. The unit supports efficient supply of multiple loads with a power envelope from 10 μW up to a short-time peak consumption of 1 W.

Furthermore, the proposed SPU provides software-configurable flexibility, including time and event management features, as required for the future generation of "always-on" intelligent IoT devices. With its size of 12 $\times$ 12 mm, it is compact in form factor despite not being fully integrated on a single die. This is achieved by the stacking of conventional printed circuit boards as shown in Fig. 3. The discrete design based on off-the-shelf components allows fast integration in IoT devices. Nevertheless, it is important to point out that the discrete design also increases costs compared to fully integrated solutions in large quantities. With a module price of 11 USD for an amount of 1000 pieces, the variable cost is high, especially compared to inductor less designs.

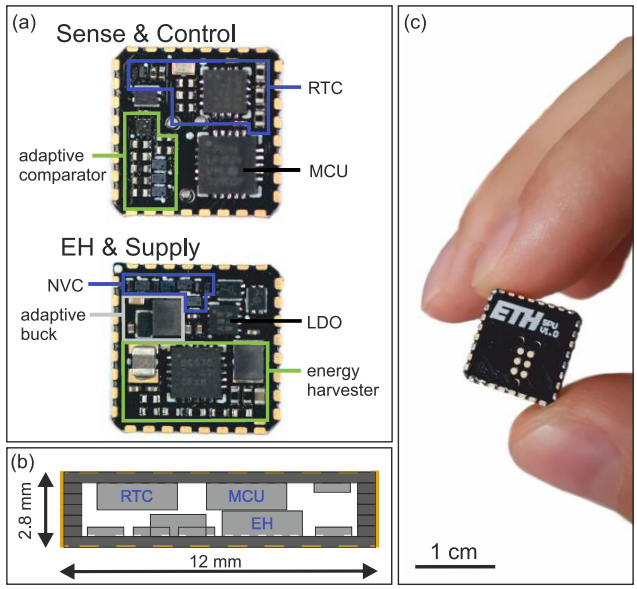

Fig. 3. Prototype of the proposed circuit in a stacked module. (a) Assembled subcircuits with highlighted functional blocks. (b) Profile illustration of the stacked module with 0.4 cm^3 volume. (c) Fully assembled module with an integrated microcontroller programming interface.

III. MODULE ARCHITECTURE

Fig. 4 illustrates the smart power unit's high-level block diagram, comprised of two subsystems: power supply with energy harvesting and software configurable power management and sensing, respectively. The module is aiming to provide power supply and harvesting at high efficiency, as well as to support a number of sleep states to trade-off responsiveness with power consumption. Subcircuits highlighted with a green triangle are directly connected to the system storage voltage VBAT, while blue marked blocks are supplied with a stabilized voltage from the linear regulator. The following subsections describe the various subcircuits, the design steps to reduce the quiescent consumption, and the configurable power modes.

A. Control and Sensing Subsystem

The control and sensing subsystem consists of three subblocks detailed below.

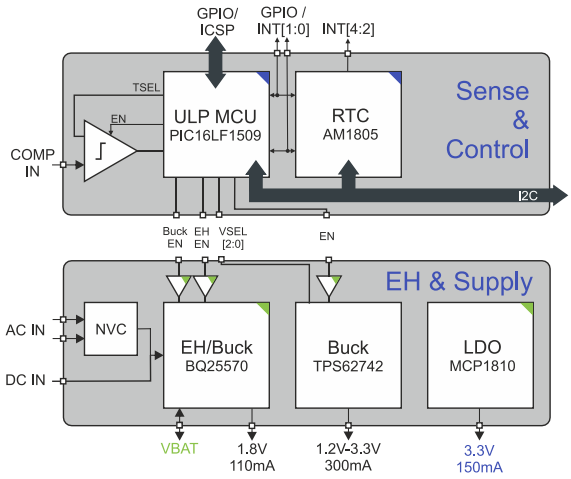

Fig. 4. High-level block diagram of the software configurable power management and supply circuit.

Ultra-low-power microcontroller: The core of the module is an 8-bit PIC16LF1509 microcontroller (MCU) with 14 kB flash memory. Its internal 31 kHz oscillator allows program execution with supply currents below 6 μA @ 3.3 V and retentive sleep at 20 nA @ 3.3 V. In addition, the MCU includes a common set of analog and digital peripherals such as analog–digital converters, digital–analog converters, and serial interfaces such as inter-integrated circuit (I2C) and universal asynchronous receiver transmitter that can be used for sensing, configuration, and data exchange.

The microcontroller's main function is to orchestrate the switching between the available power modes and thus the reduction of the quiescent current depending on the required functionality. With the flexibility of a programmable microcontroller, the module allows a fast adaption to a wide variety of wake-up sources as well as interrupts prefiltering. Furthermore, the sequence control can be implemented fully in software, and the MCU allows the offloading of lightweight background tasks from the host system. Communication with the host is performed via I2C and general purpose input–output pins (GPIOs).

Sub-threshold real-time clock: To minimize the quiescent current, the circuit uses a discrete RTC based on the Ambiq Micro AM1805. This IC is implemented in subthreshold technology, allowing time-triggered events while reducing the current consumption by 150 nA compared to the ULP-MCU's integrated RTC solutions. In fact, depending on the required accuracy, the RTC can be configured down to 14 nA @ 3.3 V. Its timekeeping features enable programmable alarms and countdowns as well as square wave generation.

Adaptable comparator: A large number of applications such as transient computing [30], EH monitoring [31], and zero-power sensing [32] benefit from a threshold-based sensing circuit to increase system sleep time without compromising latency. To support these applications, the module includes a TLV3691 comparator with an adaptable threshold. The comparator has a typical quiescent current of 75 nA @ 3.3 V, which can be eliminated with power gating if not used. To allow input signals $V_{\rm in}$ above the module voltage of 3.3 V the positive comparator

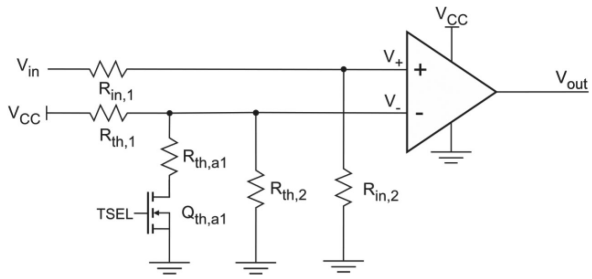

Fig. 5. Schematic of the adaptable comparator. $V_{\rm cc}$, as well as the threshold is controlled via the MCU.

input is reduced with a high-value voltage divider, $R_{\rm in,1}$ and $R_{\rm in,2}$, to keep the quiescent current low. The threshold can be adapted with a parallel connection of MOSFET switched resistors controlled via the microcontroller with TSEL as shown in Fig. 5.

B. Energy Harvesting and Power Supply Subsystem

This sub-block includes both the energy harvesting subsystems and the circuitry to supply the IoT device.

Energy harvesting circuit: This subsystem comprises an energy harvesting circuit based on the BQ25570 converter IC. Its dc–dc boost charger allows warm-start operation down to an input voltage of 100 mV. MPPT can be programmed with external resistors between 50% and 80% of the open-circuit input voltage. The EH circuit operates with common energy storage chemistries as well as super-capacitors and offers basic charge and discharge protection features. In addition to the boost converter, the IC contains a light load optimized buck converter programmed to 1.8 V output voltage with a maximal output current of 110 mA. When energy harvesting is impossible or inefficient, the whole energy harvesting circuit can be turned OFF from the microcontroller reducing its quiescent current from 488 to 4 nA.

Negative voltage converter rectifier: To extract efficiently energy from ac sources, such as piezoelectric or RF transducers, the module comprises a negative voltage convert rectifier (NVC). This circuit combines the effects of a diode full-wave rectifier (FWR) with an NVC build-out of MOSFETs, as shown in the inset of Fig. 6. [33]. For input voltages below the transistor thresholds $V_{\rm th}$, the Schottky diodes are conducting to allow low voltage operation. If the input amplitude is surpassing $V_{\rm th}$, the transistors reduce the losses caused by the diode's forward voltages. To achieve low component footprint and high efficiency the Schottky diodes DSF01S30SL for D_1-D_4, the NMOS transistors CSD13383F4 for Q_1, Q_2 and the PMOS transistors CSD23382F4 for Q_3, Q_4 have been used. The increased efficiency compared to an FWR based on similar diodes as a function of the rms input voltage is shown in Fig. 6.

The increased overall conversion efficiency comes at the cost of the missing reverse current blocking capability of the circuit [34].

Runtime adaptable buck converter: A second buck converter with peak output currents of up to 300 mA is present with the TPS62743. With its efficiency of up to 95%, it is meant to be used for an efficient supply of low voltage IoT application processors,

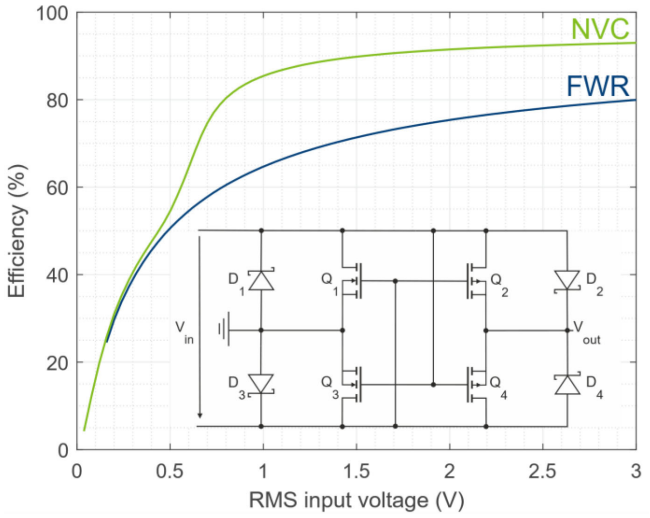

Fig. 6. Conversion efficiency of the negative voltage converter rectifier (NVC) compared to full-wave receiver (FWR) for a source impedance of 100 kΩ. The inset shows the NVC circuit consisting out of a classical FWR and a MOSFET voltage converter.

such as RISC-V based near-threshold parallel ultra-low-power processors supplied with l.2 V V_{DD} [35], as well as for RF interface circuits with supply voltages above 1.8 V . The converter output voltage can be configured at runtime between 1.2 and 3.3 V in steps of 300 mV via the microcontroller. An additional control line allows to power down the converter.

Always-ON domain: The microcontroller and the RTC have to be powered in every operational state. To achieve the lowest possible power consumption in light-load situations, these components are powered by a nA quiescent current optimized MCP1810 LDO supplied by the battery. The LDO, which can provide up to 150 mA, might be used to supply external always-ON circuitry such as volatile memory and sensors.

C. Interoperability and Integration

The limiting factor for integration and control of a complex IoT edge device is the pin count of the microcontroller. For the communication with the host system I^2C is used with the SPU acting as the bus master. The same bus also allows the extension of signal and control lines with I2C I/O expander circuits at the cost of higher quiescent consumption. Bidirectional event communication is enabled with additional interrupt lines parallel to the bus. The Circuit Serial Programming and its associated clock and data lines, which are initially used to reprogram the microcontroller, are also available as GPIOs.

On the module itself, the configuration of the RTC and its power management features is done via I2C. If the onboard RTC does not use the interrupt lines between the two subcircuits, they can be utilized by external circuitry. The control of the voltage converters and the comparator is done with GPIOs. For subcircuits directly connected to the energy storage, low-leakage load switches are used as level shifters as described in the following section, to allow a broad range of storage voltage levels.

TABLE III
QUIESCENT CURRENT DEEP SLEEP

Subsystems	DEEPSLEEP consumption V_{BAT} = 3.7 V @ 25 °C	
LDO – MCP1810	11 nA	41 nW
MCU – PIC16LF1509	15 nA	55 nW
RTC – AM1805	17 nA	63 nW
BUCK - TPS62742 with switch	7 nA	26 nW
EH – BQ25570 with switch	4 nA	15 nW
Total	54 nA	200 nW

D. Leakage Current Reduction

One of the most important lifetime constraining factors of battery-powered IoT devices is quiescent current. To minimize the quiescent current, the SPU is designed with a novel system-level power gating for every functional block, achieving a typical full system current consumption of 54 nA in deep sleep mode. This is enabled by highly optimized load switches from Vishay in combination with careful component selection. The SiP32431 with a stated quiescent current of 14 pA and a typical input leakage current of 10 pA is used when the subsequent circuit is able to compensate with its low input impedance the missing load discharge circuit. If a floating output after disabling cannot be tolerated, as it is the case for the active high enable input of the BQ25570, the SiP4282A load switch is used. It shows similar characteristics for the integrated p-channel power path transistor but with an additional load discharge circuit. The increased functionality comes at the cost of 3.5 times higher quiescent current of 50 pA. The quiescent current of the switches increases to several μA if the voltage levels of the control signals are significantly lower than the switched voltages. As a result, the systems voltage level has been set to 3.3 V to allow efficient switching of battery voltages of 4.2 V, even though this comes at the expense of a doubled current consumption of the MCU in the active state compared to 1.8 V operation.

The leakage currents in the subcircuits in the most energy-efficient configuration of DEEP SLEEP are summarized in Table III. The measurements have been conducted at room temperature with a Keysight source/measurement unit (SMU) B2912A supplying the circuit from the storage voltage pin VBAT, to reliable include all relevant losses. To identify the leakage current of every subsystem, the individual circuit parts have been iteratively assembled and characterized.

E. Power Modes

One of the most interesting features of the proposed power gating is the capability of the circuit to be configured in a variety of power modes enabling energy-efficient operation for a wide range of targeted applications. An overview of the available power modes and the corresponding active circuits is shown in Table IV:

ACTIVE – In the active mode, all subcircuits are turned ON and the MCU is running at 31 kHz, allowing reconfiguration

TABLE IV
POWER MODES OVERVIEW

Mode	VSENS	BUCK adaptive	EH	BUCK 1.8V	MCU	Power
ACTIVE	ON	ON	ON	ON	ACTIVE	21.7 µW
PM0	ON	ON	ON	ON	SLEEP	4.07 µW
PM1	OFF	ON	ON	ON	SLEEP	3.74 µW
PM2	ON	OFF	ON	OFF	SLEEP	2.56 µW
PM3	OFF	OFF	ON	ON	SLEEP	2.21 µW
PM4	OFF	OFF	ON	OFF	SLEEP	2.20 µW
PM5	OFF	ON	OFF	OFF	SLEEP	1.72 µW
SLEEP	ON	OFF	OFF	OFF	SLEEP	555 nW
DEEP SLEEP	OFF	OFF	OFF	OFF	SLEEP	200 nW

TABLE V
CURRENT CONSUMPTION

Power Mode	Current consumption I_{BAT} V_{BAT} = 3.4 V @ 25 °C	V_{BAT} = 3.7 V @ 25 °C	V_{BAT} = 4.15 V @ 25 °C
ACTIVE[a]	5.85 µA	5.87 µA	5.95 µA
PM0	1.09 µA	1.10 µA	1.19 µA
PM1	0.91 µA	1.01 µA	1.11 µA
PM2	680 nA	692 nA	732 nA
PM3	585 nA	596 nA	637 nA
PM4	585 nA	595 nA	637 nA
PM5	459 nA	464 nA	524 nA
SLEEP	147 nA	150 nA	185 nA
DEEPSLEEP	51 nA	54 nA	88 nA

[a]Microcontroller running at 31 kHz

of the circuit, communication with host devices via I2C, and simple processing tasks at a typical power consumption of 21.7 μW.

PM0 – Most of the time, the microcontroller will be configured in sleep mode which reduces the consumption by a factor of five to 4.1 μW. In this mode, all voltage regulators and the energy harvesting subcircuit are active, and the module is intended to supply the host system.

PM1 – Disabling of the threshold-based voltage sensing circuit allows to reduce the energy consumption further, depending on its voltage divider configuration, by 350 or 550 nW.

PM2 to *PM4* – Are intended for energy harvesting with a disabled adaptable buck converter. Depending on the application context, the second buck converter integrated within the energy harvesting IC, as well as the threshold-based wake-up circuit, can be deactivated.

PM5 – Powers down all circuit parts besides the adaptable buck converter. This power mode is indented for event-driven sensing with external sensors where the supply with the LDO is inefficient or impossible, as well as for memory retention of external devices.

SLEEP – The sleep mode reduces the module consumption to 555 nW (typical) while supplying the adaptable comparator to preserve the analog voltage threshold-based wake-up capability.

DEEP SLEEP – Configures the circuit into the lowest power mode where only the LDO, RTC, MCU, and load switches stay supplied. As wake-up sources, GPIO interrupts as well as timers and alarms of the subthreshold RTC can be used.

IV. EXPERIMENTAL RESULTS

Fig. 3 shows the SPU prototype developed to test functionality, power consumption, and efficiency. Static and dynamic power consumption is analyzed in subsection A. The flexibility of the MCU controlled approach to manage energy and events is shown in subsections B and C.

A. Power Consumption and Energy Harvesting Efficiency With Experimental Measurements

Table V shows the current consumption of the different power modes of the prototype. For the measurement, the storage voltage pin VBAT has been connected to a Keysight N6782A source/measurement module, and the current has been logged for different storage voltage levels to analyze the quiescent current at different battery charge states. The consumption of the circuit was measured without loads on the external supply rails at room temperature. The values have been calculated as mean out of 60 s long measurements acquired with 5 kS/s to determine the current consumption at nano-ampere precision. The used LDO regulator defines the lowest battery voltage level of 3.4 V. A battery voltage below this level will increase the regulator's static losses. Below its configured output voltage of 3.3 V, the output will follow the input voltage with a load-dependent voltage drop. The upper level is defined by the configurable overvoltage protection of the energy harvesting IC, which is typically programmed to 4.2 V. The theoretical maximal battery voltage is 5.5 V.

Fig. 7(a) Visualizes the power consumption of the circuit while switching between all available power modes supplied from a 3.7 V voltage source. The light gray trace in the background shows the measured raw data with large load changes caused by the switching of the dc/dc converters. The dark blue line indicates the average power consumption. (b) Illustrates the consumption during switching between two power modes. Depending on the capacitive load of the supplied circuits typically 100 μJ are required to change the power mode with a wake-up time of 8.15 ms.

Fig. 8 shows the EH boost converter efficiency as a function of the input voltage with a constant input current of 100 μA. For the measurement, the circuit has been configured in PM4, and the storage voltage VBAT was stabilized with a Keysight B2912A precision SMU to the characteristic values of a single-cell lithium-ion battery. The input voltage has been provided with the second channel of the SMU. Between every operation

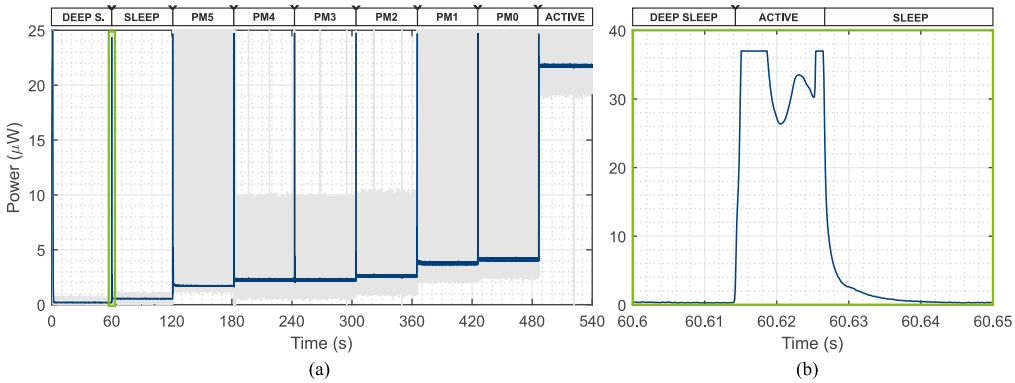

Fig. 7. (a) Power consumption of the module while switching between all available power modes controlled by an RTC timer. (b) Switching between two power modes with an energy consumption of typically 100 μJ.

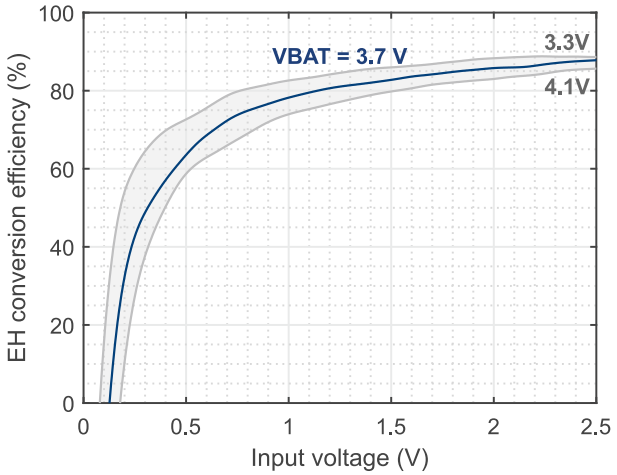

Fig. 8. EH boost conversion efficiency as a function of the input voltage with a constant input current of 100 μA.

point, the MPPT algorithm had sufficient time to find the optimal harvesting point. For a low storage voltage of 3.3 V, the circuit achieves energy neutrality from an input voltage of 100 mV with a peak conversion efficiency of 89 %. This efficiency increases with lower conversion ratios, respectively, decreases for higher conversion ratios.

B. Energy Management

To highlight the flexibility of an MCU controlled IoT power management circuit, its functionality and efficiency is analyzed in three scenarios.

Runtime voltage scaling – The adaptable buck converter allows the configuration of its output voltage at runtime via the microcontroller. This feature enables not only a simple integration of the module in circuits with different voltage requirements, but also the reduction of energy consumption through voltage scaling. In addition, it allows to reduce the component count and thus, system cost. An example of how this is applied is shown in Fig. 9(a). At $t = 0$, an interrupt event wakes-up, the system from its lowest power mode, DEEP SLEEP. The MCU sets the VSEL control lines to configure the voltage converter to an output voltage of 1.8 V, enables the circuit, and schedules a wake-up event before returning to sleep, PM5. At the subsequent wake-up, the MCU reconfigures the output voltage for 100 ms to 3.3 V and wakes-up the higher voltage load, e.g., to reach maximal transmission performance of a radio transceiver indicated with a 1 mA load current, before the system returns to its initial state, DEEP SLEEP.

High dynamic load – Fine-grain system power gating can be achieved with external load switches controlled via the microcontrollers GPIOs. For a known or MCU-managed load profile, this also allows the combination of individual voltage converters to increase the overall conversion efficiency, as shown in Fig. 9(b). This is achieved with SiP32431 load switches on the outputs of the always-ON LDO and buck converter, both configured at 3.3 V. For a storage voltage of 3.7 V and load currents below 9 μA, the LDO allows an increased supply efficiency. In the case of higher currents, the increased conversion efficiency surpasses the additional losses introduced by the active buck converter in PM5. In the analyzed operating points, the LDO and the buck converter reach a peak efficiency of 89% and 95%, respectively. It is worth noting that this efficiency break-even point is dependent on the conversion ratio. It will decrease with higher ratios by several microamperes and will significantly increase to hundreds of microamperes for lower ratios, despite the 100% duty cycle feature of the used buck converter. For applications with an unknown load profile or where the system state management is not controlled via the SPU, an additional current sensing circuit is required introducing additional losses.

Energy monitoring – The adaptable comparator allows coarse monitoring of the energy storage element and thus a system response depending on the available energy. Fig. 9(c) illustrates its usage on the example of transient computing, [30]. A 470 mF super-capacitor (Eaton KR-5R5H474-R) is connected as an energy storage element. For optimal usage of the capacitor voltage range, the battery overvoltage protection is raised from 4.2 to 5 V by replacing the corresponding voltage divider of the BQ25570 based energy harvesting subcircuit. Besides, the adaptable comparator thresholds are set to 3.7 and 4.7 V, respectively. The MCU is programmed to execute a binary state machine that enables the buck converters if the capacitor voltage (VBAT) reaches the higher *RESUME* threshold, $V_{\mathrm{TH,R}}$, and disables the converters if the lower *HIBERNATE* threshold, $V_{\mathrm{TH,H}}$, is reached.

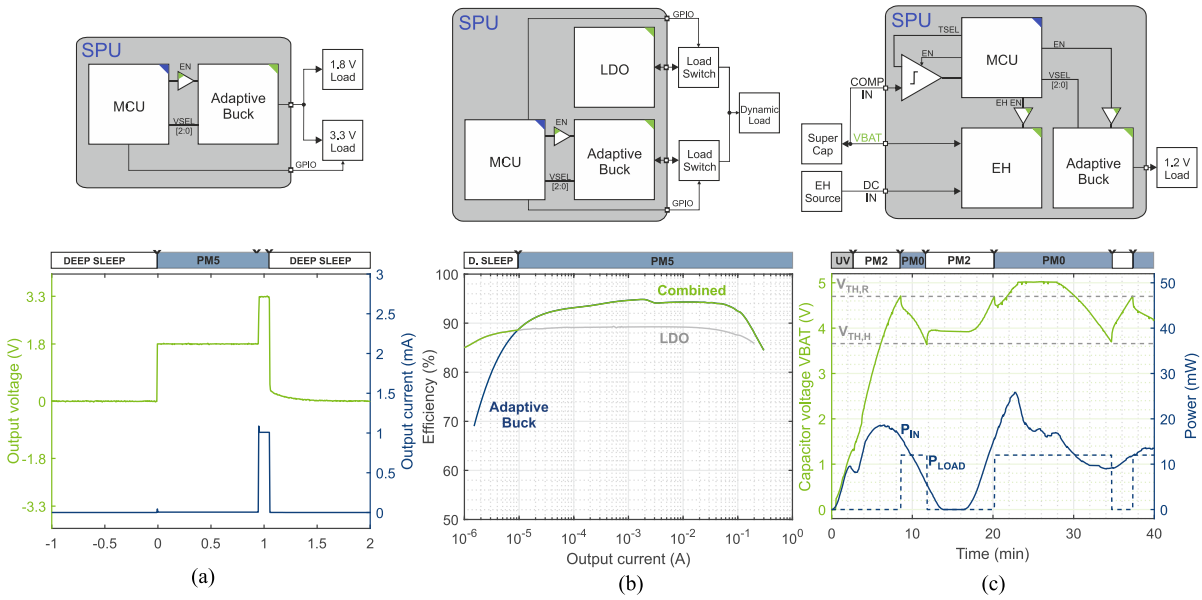

Fig. 9. Application of MCU controlled supply circuit as an extension of the proposed SPU. (a) Adaptive buck converter used to supply subsystems with a low component count efficiently. (b) Combination of always-ON LDO and adaptive buck converter for efficient supply of loads with dynamic power requirements. (c) Energy monitoring and control functionality applied to implement the concept of transient computing.

The lower plot of Fig. 9(c) shows the circuit reaction from cold-start. At $t = 0$, the capacitor is totally discharged, and the microcontroller is in an undervoltage-lockout state. Until the cold-start voltage of 0.6 V is reached, the capacitor gets directly charged from the dc_IN of the circuit. If a capacitor voltage of 0.6 V is exceeded, the boost converter and MPPT algorithm get activated, resulting in an intermediate drop of the input power. At approximately the same time at $t = 3$ min, the MCU leaves the undervoltage-lockout region, executes the boot process, schedules a wake-up event at $V_{\mathrm{TH,R}}$, and configures the circuit to PM2. Some minutes later, at $t = 8$ min, the capacitor voltage reaches the first time the upper threshold, which wakes the microcontroller. At this wake-up event, the MCU reconfigures the adaptable comparator to $V_{\mathrm{TH,H,}}$ and enables the buck converters, PM0. Subsequent follows the *RESUME* phase, where the load is supplied until the capacitor voltage drops to the *HIBERNATE* threshold, $V_{\mathrm{TH,H,}}$ and the MCU gets reactivated. Before entering the *HIBERNATE* phase, the SPU is signalizing to the host system an imminent supply shut down before the comparator gets reconfigured to $V_{\mathrm{TH,R,}}$ and the buck converters get deactivated, PM2. The switching between the two states repeats until insufficient energy is available, and an MCU undervoltage-lockout resets the sequence to its starting point. In the presented operational points, the circuit reaches an average full system efficiency of 68 % despite the large voltage conversion ratio due to the typically high capacitor voltage and the 1.2 V output voltage. The capacitor voltage graph also shows the battery overvoltage protection and the influence of the super-capacitor series resistance. At $t = 23$ min, the battery voltage rises to the maximal allowed value of 5 V, and the overvoltage protection in combination with the MPPT circuit limits the harvested power to reach an equilibrium with the consumed power. The switching between the two operational states and the accompanying 12 mW load variations results in abrupt changes of the capacitor voltage of several hundred millivolts, which must be considered for the threshold selection. For a transient system with faster response time, the storage capacity, as well as the voltage levels, can be reduced.

C. Event Management

To analyze the influence of different power management and sensing schemes, the wake-up capability from a generic voltage threshold, shown in subsection III-A, has been analyzed in terms of power consumption and latency. For the measurements, the microcontroller has been programmed to execute a binary state machine with a GPIO interrupt triggered by the comparator output (SLEEP)—event-driven—or by the RTC (DEEP SLEEP)—polling—as transition condition from sleep to the active state. In the active state, the module generates a wake-up signal for a subsequent circuit, respectively, the comparator is activated first, and the wake-up signal is generated depending on its output state. The data was acquired with a Keysight N6782A source/measurement module over 2 min at a sampling rate of 5 kS connected to the system storage voltage VBAT.

Fig. 10(a) shows the complementary cumulative distribution function (CCDF) of the different power management configurations. The CCDF illustrates the percentage of how often the power consumption exceeds a certain value and allows visualization of sparse events in a compact plot. For example, for a polling period of 1s, the microcontroller is active for 1% of the time, represented by a step between DEEP SLEEP (approx. 200 nW) and ACTIVE (approx. 20 µW) consumption shown as flat regions. The same curve shows that for 70% of the time, the consumption is below 300 nW. With longer polling periods, the active time gets reduced, as visible in the lower plateaus in the CCDF curve.

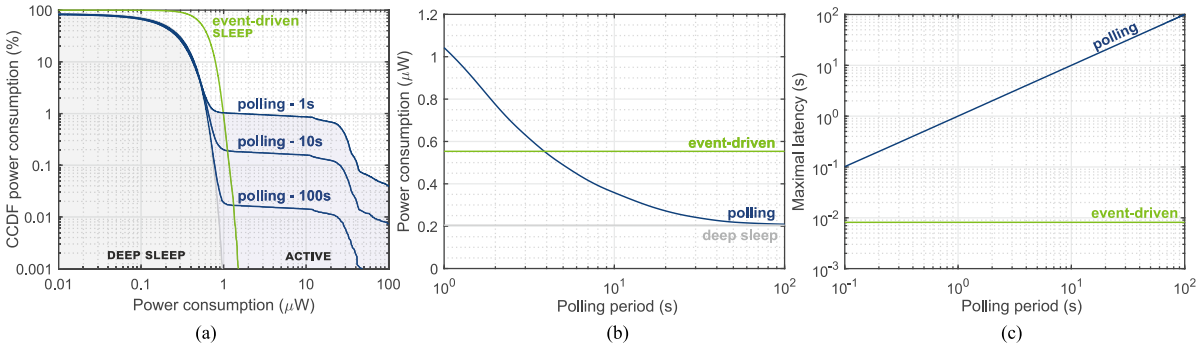

Fig. 10. Circuit power consumption with different power management schemes. (a) Complementary cumulative distribution function for polling with different polling periods and event-driven operation. (b) Power consumption as a function of the polling period. (c) Maximal latency for the generation of a wake-up pulse as a function of the polling period.

The influence of the polling rate on the average consumption is shown in Fig. 10(b). For a polling period below 4 s, the event-driven approach allows energy savings. In contrast to that for polling rates above 60 s, the total consumption is almost at the level of the leakage in the deep-sleep power mode and a further increase of the interval has a negligible influence on the total power consumption. Above 100 s, the difference in power consumption between polling and deep-sleep power mode cannot be measured reliably with the applied setup. In the event-driven configuration, the wake-up rate has a significant influence on total power consumption. For instance, the values plotted in Fig. 10(b) increase by 10 % for wake-up events every 3 s and rise further for denser wake-up events. The latency in the event-driven approach is defined by the propagation delay of the comparator and by the wake-up time of the microcontroller and has been measured at 8.15 ms as shown in Fig. 10(c). For polling, the worst-case latency of an event accruing immediately after the verification of the comparator output has to be considered. Thus, the worst-case latency is the polling period.

This evaluation of a polling and event-driven operation on the example of a generic sensor with analog output clearly shows the individual strengths and weaknesses of the two sensing paradigms. In the most extreme case of Duty Cycling, a power consumption close to the systems deep-sleep consumption can be achieved; however, at the cost of high latency and possibly lost rapid events. In contrast to that, the active detector circuit in the event-driven approach leads to a higher quiescent current, but also fewer activations of the full system, and a reduced detection latency. The inherent necessity of orders-of-magnitude lower power consumption of the always-on detector compared to the full sensing system also causes limitations of the always-on event-driven approach. Most important, a balance has to be found between the detector consumption and false-positive activations of the full sensing system. Furthermore, every missed event of the always-on detector—false-negative—leads directly to a loss of information as the entire sensing system is not activated.

V. Conclusion

This article presented the design, the implementation, and characterization of a novel smart power unit for self-sustainable IoT devices. The smart power unit has been designed for nano-quiescent current operation, proving advanced functionality such as multisource energy harvesting, software programmability, and high energy efficiency. Interfaced with the appropriate environmental source, the SPU is enabling self-sustainability for a wide range of IoT devices and applications. Experimental results have shown that the circuit allows software reconfigurable power managing and achieves a quiescent current of 54 nA during duty-cycled operation, respectively, 595 nA with active energy harvesting. The SPU has been evaluated and operates with a wide input power range of 1 μW–200 mW and allows to supply efficiently loads with dynamic power requirements. Functionality and self-sustainability have been evaluated on the example of transient computing. The event handling and its influence on power consumption were shown in a comparison between the duty cycling approach (polling) and the event-driven approach.

References

[1] D. Newell and M. Duffy, "Review of power conversion and energy management for low-power, low-voltage energy harvesting powered wireless sensors," *IEEE Trans. Power Electron.*, vol. 34, no. 10, pp. 9794–9805, Oct. 2019.

[2] C. Vanhecke *et al.*, "Multisource and battery-free energy harvesting architecture for aeronautics applications," *IEEE Trans. Power Electron.*, vol. 30, no. 6, pp. 3215–3227, Jun. 2015.

[3] "IoT: number of connected devices worldwide 2012–2025 (in billions)," Statista, 2015, Accessed: Nov. 15, 2019. lsqb;Online]. Available: https://www.statista.com/statistics/471264/iot-number-of-connected-devices-worldwide/

[4] M. H. Rehmani, M. Reisslein, A. Rachedi, M. Erol-Kantarci, and M. Radenkovic, "Integrating renewable energy resources into the smart grid: Recent developments in information and communication technologies," *IEEE Trans. Ind. Inform.*, vol. 14, no. 7, pp. 2814–2825, Jul. 2018.

[5] M. Magno and D. Boyle, "Wearable energy harvesting: From body to battery," in *Proc.12th Int. Conf. Des. Technol. Integr. Syst. Nanoscale Era*, 2017, pp. 1–6.

[6] S. M. A. Oteafy and H. S. Hassanein, "IoT in the fog: A roadmap for data-centric IoT development," *IEEE Commun. Mag.*, vol. 56, no. 3, pp. 157–163, Mar. 2018.

[7] D. Bol *et al.*, "19.6 A 40-to-80MHz Sub-4μw/mhz ULV cortex-M0 MCU SoC in 28nm FDSOI with dual-loop adaptive back-bias generator for 20μs wake-up from deep fully retentive sleep mode," in *Proc. IEEE Int. Solid-State Circuits Conf.*, Feb. 2019, pp. 322–324.

[8] A. Pullini, D. Rossi, I. Loi, G. Tagliavini, and L. Benini, "Mr.Wolf: An energy-precision scalable parallel ultra low power SOC for IoT edge processing," *IEEE J. Solid-State Circuits*, vol. 54, no. 7, pp. 1970–1981, Jul. 2019.

[9] P. Mayer, M. Magno, T. Brunner, and L. Benini, "LoRa vs. LoRa: In-field evaluation and comparison for long-lifetime sensor nodes," in *Proc. IEEE 8th Int. Workshop Adv. Sens. Interfaces*, Jun. 2019, pp. 307–311.
[10] P. Mayer, M. Magno, C. Schnetzler, and L. Benini, "EmbedUWB: Low power embedded high-precision and low latency UWB localization," in *Proc. IEEE 5th World Forum Internet Things*, Apr. 2019, pp. 519–523.
[11] B. Srbinovski, M. Magno, B. O'Flynn, V. Pakrashi, and E. Popovici, "Energy aware adaptive sampling algorithm for energy harvesting wireless sensor networks," in *Proc. IEEE Sens. Appl. Symp.*, 2015, pp. 1–6.
[12] M. Chen *et al.*, "A self-powered 3.26-μW 70-m wireless temperature sensor node for power grid monitoring," *IEEE Trans. Ind. Electron.*, vol. 65, no. 11, pp. 8956–8965, Nov. 2018.
[13] P. Mayer, M. Magno, and L. Benini, "Self-sustaining acoustic sensor with programmable pattern recognition for underwater monitoring," *IEEE Trans. Instrum. Meas.*, vol. 68, no. 7, pp. 2346–2355, Jul. 2019.
[14] M. Rusci, D. Rossi, E. Farella, and L. Benini, "A sub-mW IoT-endnode for always-on visual monitoring and smart triggering," *IEEE Internet Things J.*, vol. 4, no. 5, pp. 1284–1295, Oct. 2017.
[15] V. Jelicic *et al.*, "Towards Internet of Things for event-driven low-power gas sensing using carbon nanotubes," in *Proc. 6th Int. Workshop Adv. Sens. Interfaces*, 2015, pp. 271–276.
[16] S.-H. Chen *et al.*, "A direct AC–DC and DC–DC cross-source energy harvesting circuit with analog iterating-based MPPT technique with 72.5% conversion efficiency and 94.6% tracking efficiency," *IEEE Trans. Power Electron.*, vol. 31, no. 8, pp. 5885–5899, Aug. 2016.
[17] M. Shim, J. Jeong, J. Maeng, I. Park, and C. Kim, "Fully integrated low-power energy harvesting system with simplified ripple correlation control for system-on-a-chip applications," *IEEE Trans. Power Electron.*, vol. 34, no. 5, pp. 4353–4361, May 2019.
[18] A. Abuellil, J. J. Estrada Lopez, A. V. Bommireddipalli, A. Costilla Reyes, Z. Zeng, and E. Sanchez-Sinencio, "Multiple-input harvesting power management unit with enhanced boosting scheme for IoT applications," *IEEE Trans. Ind. Electron.*, vol. 67, no. 5, pp. 3662–3672, May 2020.
[19] A. S. Weddell, M. Magno, G. V. Merrett, D. Brunelli, B. M. Al-Hashimi, and L. Benini, "A survey of multi-source energy harvesting systems," in *Proc. Design, Automat. Test Eur. Conf. Exhib.*, 2013, pp. 905–908.
[20] D. Balsamo, M. Magno, K. Kubara, B. Lazarescu, and G. V. Merrett, "Energy harvesting meets IoT: Fuelling adoption of transient computing in embedded systems," in *Proc. IEEE 5th World Forum Internet Things (WF-IoT)*, Limerick, Ireland, 2019, pp. 413–417, doi: 10.1109/WF-IoT.2019.8767302.
[21] S. Sudevalayam and P. Kulkarni, "Energy harvesting sensor nodes: Survey and implications," *IEEE Commun. Surv. Tut.*, vol. 13, no. 3, pp. 443–461, Sep. 2011.
[22] Z. J. Chew, T. Ruan, and M. Zhu, "Power management circuit for wireless sensor nodes powered by energy harvesting: On the synergy of harvester and load," *IEEE Trans. Power Electron.*, vol. 34, no. 9, pp. 8671–8681, Sep. 2019.
[23] Q. Ju and Y. Zhang, "Predictive power management for internet of battery-less things," *IEEE Trans. Power Electron.*, vol. 33, no. 1, pp. 299–312, Jan. 2018.
[24] G. Shi *et al.*, "An efficient power management circuit based on quasi maximum power point tracking with bidirectional intermittent adjustment for vibration energy harvesting," *IEEE Trans. Power Electron.*, vol. 34, no. 10, pp. 9671–9685, Oct. 2019.
[25] D. El-Damak and A. P. Chandrakasan, "Solar energy harvesting system with integrated battery management and startup using single inductor and 3.2nW quiescent power," in *Proc. Symp. VLSI Circuits (VLSI Circuits)*, Kyoto, 2015, pp. C280–C281, doi: 10.1109/VLSIC.2015.7231290.
[26] G. Chowdary, A. Singh, and S. Chatterjee, "An 18 nA, 87% efficient solar, vibration and RF energy-harvesting power management system with a single shared inductor," *IEEE J. Solid-State Circuits*, vol. 51, no. 10, pp. 2501–2513, Oct. 2016.
[27] M. Dini, A. Romani, M. Filippi, and M. Tartagni, "A nanocurrent power management IC for low-voltage energy harvesting sources," *IEEE Trans. Power Electron.*, vol. 31, no. 6, pp. 4292–4304, Jun. 2016.
[28] M. A. Abouzied, H. Osman, V. Vaidya, K. Ravichandran, and E. Sanchez-Sinencio, "An integrated concurrent multiple-input self-startup energy harvesting capacitive-based DC adder combiner," *IEEE Trans. Ind. Electron.*, vol. 65, no. 8, pp. 6281–6290, Aug. 2018.
[29] S. S. Amin and P. P. Mercier, "MISIMO: A multi-input single-inductor multi-output energy harvesting platform in 28-nm FDSOI for powering net-zero-energy systems," *IEEE J. Solid-State Circuits*, vol. 53, no. 12, pp. 3407–3419, Dec. 2018.
[30] D. Balsamo, A. S. Weddell, G. V. Merrett, B. M. Al-Hashimi, D. Brunelli, and L. Benini, "Hibernus: Sustaining computation during intermittent supply for energy-harvesting systems," *IEEE Embedded Syst. Lett.*, vol. 7, no. 1, pp. 15–18, Mar. 2015.
[31] M. Thielen, L. Sigrist, M. Magno, C. Hierold, and L. Benini, "Human body heat for powering wearable devices: From thermal energy to application," *Energy Convers. Manage.*, vol. 131, pp. 44–54, Jan. 2017.
[32] J. Kimionis *et al.*, "Zero-power sensors for smart objects: Novel zero-power additively manufactured wireless sensor modules for IoT applications," *IEEE Microw. Mag.*, vol. 19, no. 6, pp. 32–47, Sep./Oct. 2018.
[33] A. Romani, M. Filippi, M. Dini, and M. Tartagni, "A Sub-μ a stand-by current synchronous electric charge extractor for piezoelectric energy harvesting," *ACM J. Emerg. Technol. Comput. Syst.*, vol. 12, no. 1, pp. 1–17, Aug. 2015.
[34] T. Hehn and Y. Manoli, *CMOS Circuits for Piezoelectric Energy Harvesters*, vol. 38. Dordrecht, The Netherlands: Springer, 2015.
[35] M. Eggimann, S. Mach, M. Magno, and L. Benini, "A RISC-V based open hardware platform for always-on wearable smart sensing," in *Proc. IEEE 8th Int. Workshop Adv. Sens. Interfaces*, 2019, pp. 169–174.

Philipp Mayer (Student Member, IEEE) received the B.Sc. degree from the TU Wien, Vienna, Austria, in 2016, and the consecutive M.Sc. degree from the ETH Zurich, Zurich, Switzerland, in 2018, both in electrical engineering and information technology. He is currently working toward the Ph.D. degree at the Integrated System Laboratory, ETH Zurich.

His research interests include low-power system design, energy harvesting, and edge computing.

Mr. Mayer is the recipient of the Best Paper Award at the 2017 IEEE International Workshop on Advances in Sensors and Interfaces and the Best Student Paper Award at the 2018 IEEE Sensors Applications Symposium. Beyond his particular area of expertise, he was the recipient of the Best Poster Award in the 2018 IOP Workshop in Devices, Materials and Structures for Energy Harvesting and Storage. In 2019, he founded Mayer Engineering and Consulting, intending to connect academic with industrial expertise.

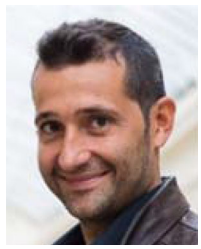

Michele Magno (Senior Member, IEEE) received the master's and Ph.D. degrees in electronic engineering from the University of Bologna, Bologna, Italy, in 2004 and 2010, respectively.

He is currently a Senior Researcher with ETH Zurich, Zurich, Switzerland, and Head of the Project-Based Learning Center with ETH Zurich. He has collaborated with several universities and research centers, such as Mid University Sweden, where he is a Guest Full Professor. He has authored/coauthored more than 150 papers in international journals and conferences, in which he got multiple best paper and best poster awards. His research interests include wireless sensor networks, wearable devices, machine learning at the edge, energy harvesting, power management techniques, and extended lifetime of batteries operated devices.

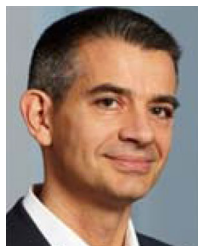

Luca Benini (Fellow, IEEE) received the Ph.D. degree in electrical engineering from Stanford University, Stanford, CA, USA, in 1997.

He has served as the Chief Architect of the Platform 2012/STHORM Project with STMicroelectronics, Grenoble, France, from 2009 to 2013. He is currently the Chair of Digital Circuits and Systems with ETH Zurich, Zurich, Switzerland, and is a Full Professor with the University of Bologna, Bologna, Italy. He has authored/coauthored more than 1000 peer-reviewed articles and five books. His research interest includes energy-efficient computing systems design from embedded to high performance.

Dr. Benini is a fellow of ACM and a member of the Academia Europaea. He was a recipient of the 2016 IEEE CAS Mac Van Valkenburg Award and the 2019 IEEE TCAD Donald O. Pederson Best Article Award.